By considering the energetics of the wollastonite model in terms of the interactions between stacking operators we have been able to show that the model possesses two important features:

(1). The interaction represented by J_4 does include a contribution from the configuration of the layers between the jth and $(j+3)$rd neighbour layers.

(2). The association of spins with layer position used in the body of the paper suggests that $|\mathbf{G}|$ must be one half of a lattice vector, but the derivation in terms of operators places no such constraint upon the magnitude of the displacement associated with the glide operator **G**. This justifies the use of the wollastonite model in systems such as zoisite where $G = 1/4[001]$.

References

ANGEL, R. J. (1985). *Mineral. Mag.* **49**, 37-48.
BAK, P. (1982). *Rep. Prog. Phys.* **45**, 587-629.
CHISHOLM, J. E. (1979). *EMAG* 1979, edited by T. MULVEY, pp. 109-112. Bristol and London: The Institute of Physics.
DOLLASE, W. A. (1968). *Am. Mineral.* **53**, 1882-1898.
DUXBURY, P. M. & SELKE, W. (1983). *J. Phys. A: Gen. Phys.* **16**, L741-L744.
ELLIOT, R. J. (1961). *Phys. Rev.* **124**, 346-353.
FISHER, M. E. & SELKE, W. (1980). *Phys. Rev. Lett.* **44**, 1502-1505.
FISHER, M. E. & SELKE, W. (1981). *Philos. Trans. R. Soc. London Ser. A*, **302**, 1-44.
FRANK, F. C. (1951). *Philos. Mag.* **42**, 1014-1021.
GARD, J. A. (1966). *Nature (London)*, **211**, 1078-1079.
GARD, J. A. & TAYLOR, H. F. W. (1960). *Acta Cryst.* **13**, 785-793.
GUGGENHEIM, S. (1978). *Am. Mineral.* **63**, 1260-1263.
GUINIER, A., BOKIJ, G. B., BOLL-DORNBERGER, K., COWLEY, J. M., ĐUROVIČ, S., JAGODZINSKI, H., KRISHNA, P., DE WOLFF, P. M., ZVYAGIN, B. B., COX, D. E., GOODMAN, P., HAHN, TH., KUCHITSU, K. & ABRAHAMS, S. C. (1984). *Acta Cryst.* A**40**, 399-404.
HENMI, C., KAWAHARA, A., HENMI, K., KUSACHI, I. & TAKEUCHI, Y. (1983). *Am. Mineral.* **68**, 156-163.
HENMI, C., KUSACHI, I., KAWAHARA, A. & HENMI, K. (1978). *Mineral. J.* **9**, 169-178.
ITO, T. (1950). *X-ray Studies on Polymorphism.* Tokyo: Maruzen.
JAGODZINSKI, H. (1954). *Neues Jahrb. Mineral. Monatsh.* **3**, 49-65.
JEFFERSON, D. A. & BOWN, M. G. (1973). *Nature (London)*, **245**, 43-44.
JENKINS, D. M., NEWTON, R. C. & GOLDSMITH, J. R. (1983). *Nature (London)*, **304**, 622-623.
JEPPS, N. W. & PAGE, T. F. (1983). *J. Cryst. Growth Charact.* **7**, 259-308.
KUDOH, Y. & TAKEUCHI, Y. (1979). *Mineral. J.* **9**, 349-373.
MAMEDOV, KH. & BELOV, N. V. (1956). *Zap. Vses. Mineral. Ova*, **85**, 13-38.
MULLER, W. F. (1976). *Z. Kristallogr.* **144**, 401-408.
PREWITT, C. T. & BUERGER, M. J. (1963). *Mineral. Soc. Am. Spec. Pap.* I, pp. 293-302.
PRICE, G. D. (1983). *Phys. Chem. Miner.* **10**, 77-83.
PRICE, G. D., PARKER, S. C. & YEOMANS, J. (1985). *Acta Cryst.* B**41**, 231-239.
PRICE, G. D. & YEOMANS, J. (1984). *Acta Cryst.* B**40**, 448-453.
RAY, N., PUTNIS, A. & GILLET, P. (1985). In preparation.
SMITH, J., YEOMANS, J. & HEINE, V. (1984). *Proceedings of the NATO Advanced Studies Institute on Modulated Structure Materials*, edited by T. TSAKALAKOS, p. 95. Dordrecht: Nijhoff.
THOMPSON, J. B. (1981). *Structure and Bonding in Crystals.* II, edited by M. A. O'KEEFFE and A. NAVROTSKY, pp. 168-196. New York: Academic Press.
WELTNER, W. (1969). *J. Chem. Phys.* **51**, 2469-2483.
WENK, H.-R. (1969). *Contrib. Mineral Petrol.* **22**, 238-247.

Acta Cryst. (1985). B**41**, 319-329

A Structure Classification of Symmetry-Related Perovskite-Like ABX_4 Phases*

BY R. DEBLIECK, G. VAN TENDELOO, J. VAN LANDUYT AND S. AMELINCKX†

University of Antwerp (RUCA), Groenenborgerlaan 171, *B*-2020 *Antwerp, Belgium*

(*Received* 18 *February* 1985; *accepted* 16 *May* 1985)

Abstract

An exhaustive count is performed of all possible perovskite-like ABX_4 phases, with the assumption that the only occurring symmetry-reducing operation is the tilting of regular BX_6 octahedra. Each structure is schematically represented and is fully determined by its structure symbol, the space group and the diffraction features, which are condensed in a powerful shorthand notation: the 'diffraction typology'. Attention is paid to the displacement of the A cation and the resulting antiferroelectricity. The interrelations between the structures are presented in the 'family tree' formalism in order to provide insight concerning the group-to-subgroup relations as a helpful tool in the prediction of phase transitions.

1. Introduction

Perovskites with general structure formula ABX_3 such as $SrTiO_3$ and $NaNbO_3$ undergo phase transitions featuring the condensation of soft phonon modes upon lowering the temperature (Ahtee, Glazer & Megaw, 1972; Kay & Bailey, 1957). The perovskite-like ABX_4 compounds such as $RbVF_4$ and $RbFeF_4$ have a basic structure that is very similar to the basic ABX_3 structure as can be seen by comparison of Figs. 1(*a*) and 1(*b*): in the ABX_4 case the BX_6 octahedra are only two-dimensionally corner linked, thus form-

* Work performed under the auspices of association SCK-RUCA and with financial help from IIKW.

† Also at: SCK/CEN, B-2400 Mol, Belgium.

0108-7681/85/050319-11$01.50

ing mechanically independent layers of octahedral networks. Nevertheless, the ABX_4 compounds still undergo phase transitions involving condensation of soft modes, which makes them very interesting examples of transitions in systems with reduced dimensionality.

In general, phase transitions can be interpreted as symmetry reductions that are best represented by the group-to-subgroup relation between the respective space groups belonging to the structures of the phases involved in the transition. Because the knowledge of these relations between the phases of a particular compound is of great importance for the understanding of the mechanisms of the transitions, the group-to-subgroup relations will be outlined for all derived ABX_4 phases.

Megaw (1973) introduced the concept 'aristotype' for the phase with the highest possible symmetry and the phases derived from it by the proper symmetry reductions are designated 'hettotypes'. This nomenclature will be used henceforth.

Glazer (1972) pointed out that the most important mechanism of symmetry reduction during the transitions in ABX_3 compounds results from the tilting of rigid BX_6 octahedra. This is feasible because the lattice modes that become unstable upon lowering the temperature such as the M_3 and the R_{25} zone-boundary modes (representation when the origin is chosen on the A-cation position) have low frequencies and feature the in-phase oscillation of complete undistorted octahedra. Moreover it is generally found that the observed space group is identical with the space group of the tilted octahedral framework and hence remains centrosymmetric.

The similarity of the ABX_3 and the ABX_4 aristotype structures and the occurrence of the same type of transitions in both cases suggest that here too the most important symmetry reductions will arise from the tilting of the regular octahedra. This is confirmed by many experimental facts (Abrahams & Bernstein, 1972; Babel, Wall & Heger, 1974; Hidaka, Wood & Garrard, 1979; Hidaka, Wood, Wanklyn & Garrard, 1979; Hidaka, Wood & Wondre, 1979; Hidaka, Inoue, Garrard & Wanklyn, 1982; Bulou, Fourquet, Leble, Nouet, De Pape & Plet, 1983).

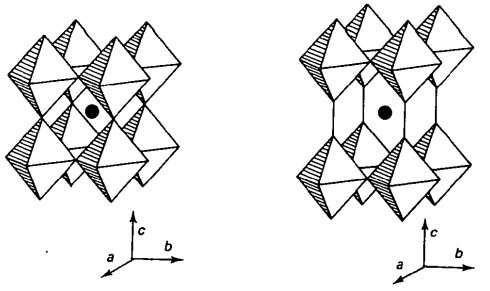

(a) (b)

Fig. 1. The aristotype structures of (a) ABX_3; (b) ABX_4. The BX_6 octahedra are hatched, the black circle is the A cation.

The purpose of this paper is to provide a complete classification of the ABX_4 hettotypes involving the tilting of regular octahedra. Also some attention is paid to the displacement of the A cation, which may give rise to either a ferro- or an antiferroelectric phase, depending on whether the symmetry reduction leads to a polar or a nonpolar subgroup.

2. Structure symbol for the condensed modes

(a) ABX_3 structures

As previously mentioned the structures of the low-temperature phases when their symmetry is reduced through the condensation of a soft phonon can be interpreted in terms of the tilting of regular BX_6 octahedra with respect to their orientation in the aristotype structure shown in Fig. 1(a). How the tilting looks when a particular tilting scheme (indicated) is applied to the octahedra forming (001) layers is shown in Fig. 2. This tilting scheme can be broken down into component tilts around the tetrad axes of the octahedra and from Fig. 1(a) it is clear that these tetrad axes are directed along the basic translations of the perovskite lattice.

Obviously a symbolic structure notation able to discern between the possible hettotypes must contain information about the tilting magnitude around each axis and indicate whether tilting is present or not. Furthermore, since zone-boundary modes are considered and the new lattice period is never more than two basic periods, this notation must also reveal whether the tilting sense along an axis is alternating or not. This feature will henceforth be designated as 'tilt correlation' along an axis.

Glazer (1972) proposed the following general notation for the ABX_3 structure, which seems appropriate because it is clear, concise and contains all the necessary information pointed out in the preceding paragraph:

$$\mathbf{a}^i\mathbf{b}^j\mathbf{c}^k. \qquad (1)$$

The first, second and third positions of this structure symbol contain information about the crystallographic [100], [010] and [001] axes respectively. The letters **a**, **b** and **c** denote that the tilting magnitudes around each of the axes are different; whenever the tilting magnitudes around two or more axes are equal

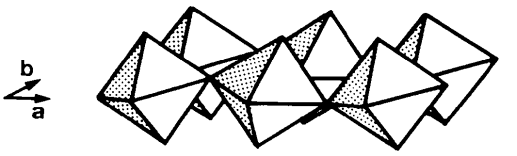

Fig. 2. Tilting of regular BX_6 octahedra in the (001) layer in ABX_3 and ABX_4 compounds. The tilting here would be described as $\mathbf{a}^0\mathbf{a}^+\mathbf{a}^0$.

Table 1. *List of the 23 possible ABX_3 structures as derived by Glazer* (1972, 1975)

The structure symbol is accompanied by an appropriate specification of the unit-cell characteristics. The subscript p used for the unit-cell multiplicity stands for 'pseudocubic' referring to the formerly cubic axes.

Serial number	Symbol	Lattice centring	Multiple cell	Relative pseudocubic subcell parameters	Space group
Three-tilt systems					
(1)	$a^+b^+c^+$	I	$2a_p \times 2b_p \times 2c_p$	$a_p \neq b_p \neq c_p$	$Immm$ (No. 71)
(2)	$a^+b^+b^+$	I		$a_p \neq b_p = c_p$	$Immm$ (No. 71)
(3)	$a^+a^+a^+$	I		$a_p = b_p = c_p$	$Im3$ (No. 204)
(4)	$a^+b^+c^-$	P		$a_p \neq b_p \neq c_p$	$Pmmn$ (No. 59)
(5)	$a^+a^+c^-$	P		$a_p = b_p \neq c_p$	$Pmmn$ (No. 59)
(6)	$a^+b^+c^-$	P		$a_p \neq b_p = c_p$	$Pmmn$ (No. 59)
(7)	$a^+a^+a^-$	P		$a_p = b_p = c_p$	$Pmmn$ (No. 59)
(8)	$a^+b^-c^-$	A		$a_p \neq b_p \neq c_p$ $\alpha \neq 90°$	$A2_1/m11$ (No. 11)
(9)	$a^+a^-c^-$	A		$a_p = b_p \neq c_p$ $\alpha \neq 90°$	$A2_1/m11$ (No. 11)
(10)	$a^+b^-b^-$	A		$a_p \neq b_p = c_p$ $\alpha \neq 90°$	$Pmnb$ (No. 62)*
(11)	$a^+a^-a^-$	A		$a_p = b_p = c_p$ $\alpha \neq 90°$	$Pmnb$ (No. 62)*
(12)	$a^-b^-c^-$	F		$a_p \neq b_p \neq c_p$ $\alpha \neq \beta \neq \gamma \neq 90°$	$F\bar{1}$ (No. 2)
(13)	$a^-b^-b^-$	F		$a_p \neq b_p = c_p$ $\alpha \neq \beta \neq \gamma \neq 90°$	$I2/a$ (No. 15)*
(14)	$a^-a^-a^-$	F		$a_p = b_p = c_p$ $\alpha = \beta = \gamma \neq 90°$	$R\bar{3}c$ (No. 167)
Two-tilt systems					
(15)	$a^0b^+c^+$	I	$2a_p \times 2b_p \times 2c_p$	$a_p < b_p \neq c_p$	$Immm$ (No. 71)
(16)	$a^0b^+b^+$	I		$a_p < b_p = c_p$	$I4/mmm$ (No. 139)
(17)	$a^0b^+c^-$	B		$a_p < b_p \neq c_p$	$Bmmb$ (No. 63)
(18)	$a^0b^+b^-$	B		$a_p < b_p = c_p$	$Bmmb$ (No. 63)
(19)	$a^0b^-c^-$	F		$a_p < b_p \neq c_p$ $\alpha \neq 90°$	$F2/m11$ (No. 12)
(20)	$a^0b^-b^-$	F		$a_p < b_p = c_p$ $\alpha \neq 90°$	$Imcm$ (No. 74)*
One-tilt systems					
(21)	$a^0a^0c^+$	C	$2a_p \times 2b_p \times c_p$	$a_p = b_p < c_p$	$C4/mmb$ (No. 127)
(22)	$a^0a^0c^-$	F	$2a_p \times 2b_p \times 2c_p$	$a_p = b_p < c_p$	$F4/mmc$ (No. 140)
Zero-tilt system					
(23)	$a^0a^0a^0$	P	$a_p \times b_p \times c_p$	$a_p = b_p = c_p$	$Pm3m$ (No. 221)

* These space-group symbols refer to axes chosen according to the matrix transformation

$$\begin{pmatrix} 1 & 0 & 0 \\ 0 & \frac{1}{2} & -\frac{1}{2} \\ 0 & \frac{1}{2} & \frac{1}{2} \end{pmatrix}.$$

this is denoted by a repetition of the same letter. The superscripts i, j, k can be 0, + or − depending on the tilt correlation. If the tilt correlation is positive, alternate octahedra along the considered axis have the same sense of tilting whereas a negative tilt correlation indicates that alternate octahedra are tilted in the opposite sense. Zero tilt correlation clearly indicates that no tilting at all has occurred around the considered axis.

The effects of tilting on the periodicity are obvious. Tilting around one axis will automatically double the periodicity along the perpendicular axes, whereas negative tilt correlation will also double the periodicity along the considered axis.

Any kind of tilting will also result in a decrease of the distances between the centres of the octahedra along the axes perpendicular to the tilt axis and in the case where negative correlation occurs along more than one axis, the interaxial angles will also be affected, giving rise to monoclinic or triclinic unit cells.

In any case the structure symbol (1) described above establishes the structure of a condensed mode unambiguously.

Table 1 shows the 23 possible phases of the ABX_3 structure, indicated by their structure symbol together with the space group, the unit-cell multiplicity and centring with respect to the aristotype unit cell, as derived by Glazer (1972, 1975).

(*b*) *Extension for ABX_4 structures*

It is clear from Fig. 1(*b*) representing the aristotype structure of the ABX_4 compounds that some mechanical constraints are lost because vertex linking of the octahedra is restricted to the (001) planes. Nevertheless, similar phase transitions involving the condensation of zone-boundary soft phonons still occur.

Here too the most important parameter involved in the soft modes is tilting of the octahedra and the possible concomittant displacement of the A cations. As for the displacement of the B cations, distortions of the octahedra are normally second-order effects; furthermore, it was found in $RbFeF_4$ and $CsFeF_4$ that the Fe^{3+} cations are not displaced during the transition (Abrahams & Bernstein, 1972). As can be seen upon inspection of Table 3, the observed space groups are generally identical with the space groups of the tilted octahedral framework. Therefore the tilting of octahedra will be considered as the unique symmetry-reducing mechanism.

Consequently the ABX_3 structure symbol (1) is often, although erroneously, used to describe the

ABX_4 hettotype structures (Hidaka, Wood & Garrard, 1979; Hidaka, Wood, Wanklyn & Garrard, 1979; Hidaka, Wood & Wondre, 1979; Hidaka *et al.*, 1982). The same notation should not be used since, obviously, the gain of degrees of freedom in the ABX_4 case will make the ABX_3 description degenerate. Indeed, when a particular ABX_3 tilting scheme is applied to the ABX_4 case, one still has liberty to choose whether the tilt around the [100] or the [010] axis will be parallel or antiparallel in the alternate (001) layers.

It is therefore suggested (Bulou *et al.*, 1983) that the ABX_3 structure symbol (1) should be extended with two subscripts so as to account for the supplementary degrees of freedom. The structure symbol for the ABX_4 structure then becomes

$$\mathbf{a}_u^i\mathbf{b}_v^j\mathbf{c}^k, \qquad (2)$$

where the subscripts u, v indicate whether the tilt around [100] or [010] is parallel (p) or antiparallel (a) in the alternate (001) layers. So u, v can be either a or p, covering all possible hettotypes for the ABX_4 case.

(c) *Calculation of the superstructure reflections*

Because the number of possible hettotypes is tremendous when compared with the ABX_3 case, our first aim is a computer generation of the structures, in order to calculate which superstructure reflections will be present.

(i) *Tilting of the octahedra.* The octahedra of the undistorted idealized ABX_4 structure from Fig. 1(b) must be tilted according to a particular tilting scheme, but in order to do so three rotation operations around the tetrad axes must be performed.

Here a note of caution must be sounded: the commutator of two rotation operations R_1 and R_2 is in general nonzero:

$$[R_1, R_2] \neq 0,$$

which means that the final orientation of the octahedra will depend on the order of application of the rotation operations. It is, however, easy to prove that for small tilt angles (it is experimentally found that 10° is seldom exceeded) the influence of the sequence of the rotations on the resulting orientation is a second-order effect and can be neglected.

Using the above approximation and rotating counterclockwise the transformation matrix for the tilting of the first octahedron reads:

$$\begin{bmatrix} 1 & \gamma & -\beta \\ -\gamma & 1 & \alpha \\ \beta & -\alpha & 1 \end{bmatrix}, \qquad (3)$$

where α, β and γ are the tilt angles around the [100], [010] and [001] axes respectively.

Since only doubling of the periodicity along each axis is allowed, a superstructure unit cell containing eight octahedra will suffice for the description.

The transformation matrices for the tilting of the seven remaining octahedra are to be determined from the considered structure symbol (2).

(ii) *Displacement of the A cations.* Comparison with experimental results in the literature shows that sometimes more superstructure reflections occur than can be explained by mere octahedral tilt. As was already pointed out the most feasible additional distortion is the displacement of the A cation.

In order to calculate this displacement due to the configurational change during the phase transition, the interaction between the considered cation and its nearest neighbours has to be known at least qualitatively.

The octahedral tilt will distort the arrangement of the neighbouring X anions, thus disturbing the potential hypersurface and forcing the A cation to a new equilibrium position. A pair potential of the type Coulomb-Born-Mayer is used to describe all interactions between the A^+ cation and its nearest neighbours:

$$V(\varepsilon, \eta, \xi) = \sum_{i=1}^{N} Z_i e^2 / R_i(\varepsilon, \eta, \xi) + A_i \exp[-R_i(\varepsilon, \eta, \xi)/\rho_i] \qquad (4)$$

with

$$R_i(\varepsilon, \eta, \xi) = [(x_i - \varepsilon)^2 + (y_i - \eta)^2 + (z_i - \xi)^2]^{1/2},$$

whereby N is the number of neighbours, (x_i, y_i, z_i) the position of the ith ion and (ε, η, ξ) the displacement of the cation; R_i, A_i and ρ_i are respectively the distance and the Born-Mayer interaction parameters between the A cation and the ith surrounding ion and Z_i is the charge of the ith ion.

The total number of neighbours accounted for is 34, including 16 X^-, eight B^{3+} ions and ten A^+ ions. In a first-order approximation the surrounding A^+ ions are considered as fixed. The Born-Mayer interaction parameters were taken from the literature (Gupta, Pande, Shukla & Sharma, 1980; Upadhyaya, Wang & Moore, 1980). A variational procedure to determine ε, η and ξ causes numerical problems; therefore a gradient algorithm was applied. The resulting displacements, if any, are typically about 0·1 to 0·2 Å.

It is obvious that there must exist an unambiguous relationship between this displacement and the occurrence of ferro- or antiferroelectric phases. Therefore the dipole moments of the eight original aristotype subcells contained in the considered superstructure unit cell are calculated in order to reveal possible ferro- and antiferroelectric phases. Since the applied symmetry reduction conserves the centre of sym-

metry, the space group of the generated hettotypes being nonpolar, the only phases featuring subcell dipoles must be antiferroelectric.

The resulting dipole moments, if any, amount to between $0{\cdot}33\times10^{-30}$ and $4{\cdot}3\times10^{-30}$ Cm for the case of $RbVF_4$ with tilt angles of $\alpha=6$, $\beta=7{\cdot}2$ and $\gamma=9°$, but generally 10×10^{-30} to 16×10^{-30} Cm is found.

3. The complete list of all possible ABX_4 structures

Exhaustive application of all degrees of freedom of the structure symbol yields 74 different hettotype structures. It must be emphasized that structures that turn out to be equivalent after the proper rotation have been omitted. Indeed, it should be clear that the structures of type

$$\mathbf{a}_a^+\mathbf{b}_p^+\mathbf{c}^0 \quad \text{and} \quad \mathbf{a}_p^+\mathbf{b}_a^+\mathbf{c}^0$$

are equivalent and can be matched when either one is rotated over $\pi/2$ around [001] and as a consequence only one of them is to appear in the complete list.

(*a*) *Schematic representation*

A schematic representation of the 45 different structures, occurring when differences in tilting magnitudes are neglected, is shown in Fig. 3; the magnitude indications **a**, **b**, **c** of the structure symbol (2) have been omitted because of this neglect.

This schematic representation is sufficient for the determination of the space groups of all occurring hettotype phases.

(*b*) *Diffraction typology*

For the sake of clarity and conciseness the results of the computer calculations will be abbreviated in a useful code, which will henceforth be called the

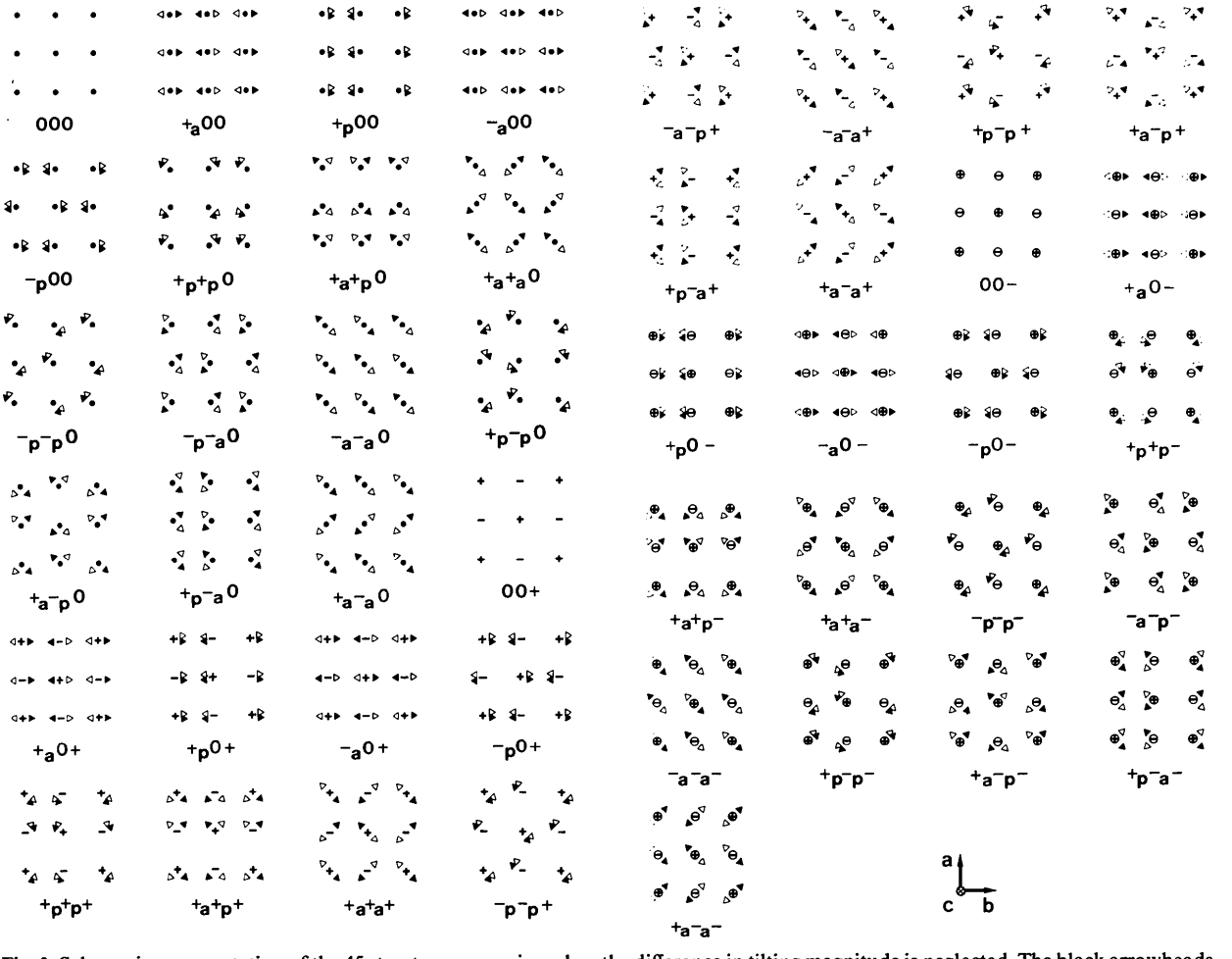

Fig. 3. Schematic representation of the 45 structures occurring when the difference in tilting magnitude is neglected. The black arrowheads indicate the displacement of the top vertices of the octahedra in one (001) layer, whereas the white arrowheads indicate displacements in the next layer. Dots, plus and minus signs represent the tilting sense around [001] where a dot indicates that there is no tilting and the signs indicate tilting in an opposite sense. Encircled signs stand for negative tilt correlation along [001]. The structure symbol is somewhat simplified because tilting magnitudes were neglected.

'diffraction typology'. All indices of occurring reflections will be referred to a superstructure unit cell, whereby the original aristotype unit cell is double along each of its three basic crystallographic axes.

The various types of reflections are then indicated using the following Brillouin-zone notation, where the letter *u* (*ungerade*) indicates an odd index whereas the letter *g* (*gerade*) indicates an even index.

$$F = ggg \qquad A = uuu$$
$$X = ugg \qquad R = ugu$$
$$Y = gug \qquad S = guu$$
$$Z = ggu \qquad M = uug.$$

F represents the basic structure reflections and *X*, *Y*, *Z*, *A*, *R*, *S* and *M* are superstructure reflections occurring at zone boundaries, as is illustrated in Fig. 4.

This code will provide a powerful shorthand representation of the reflections occurring in a particular phase, by simply stating which types of reflections are not systematically absent.

Because the presence of the basic structure reflections *F* is trivial they will be omitted.

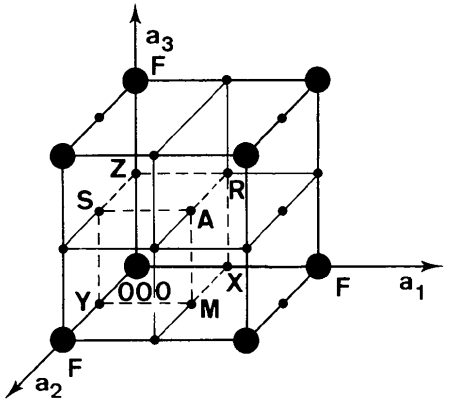

Fig. 4. The Brillouin-zone code used for the diffraction typology.

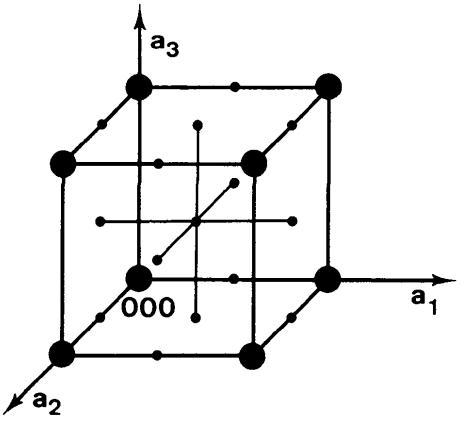

Fig. 5. Example of diffraction typology showing which superstructure reflections are not systematically absent for the case *AXYRSM*.

For example: the phase with its structure represented by the symbol

$$\mathbf{a}_p^+\mathbf{b}_p^+\mathbf{c}^- \ (Pmmn)$$

has a diffraction typology *AXYRSM*, which is represented schematically in Fig. 5. This is of course a tremendous simplification of the very extensive results, but complete structure-factor listings are obtainable from the authors.

(*c*) *Antiferroelectricity*

As pointed out before, the phases featuring subcell dipoles must be antiferroelectric. The arrangement of the dipoles in these antiferroelectric phases is best expressed by a schematic drawing whereby the dipoles are represented by arrows. This is done in Fig. 6 where the dipole configurations resulting from the application of some experimentally observed tilting schemes are displayed. Other results will not be presented here for the sake of conciseness. It must be remarked that sometimes more than one type of dipole is found within one phase. Indeed, when more than one magnitude of *A* cation displacement is found it is generally expected that as many dipole types as displacement types will occur.

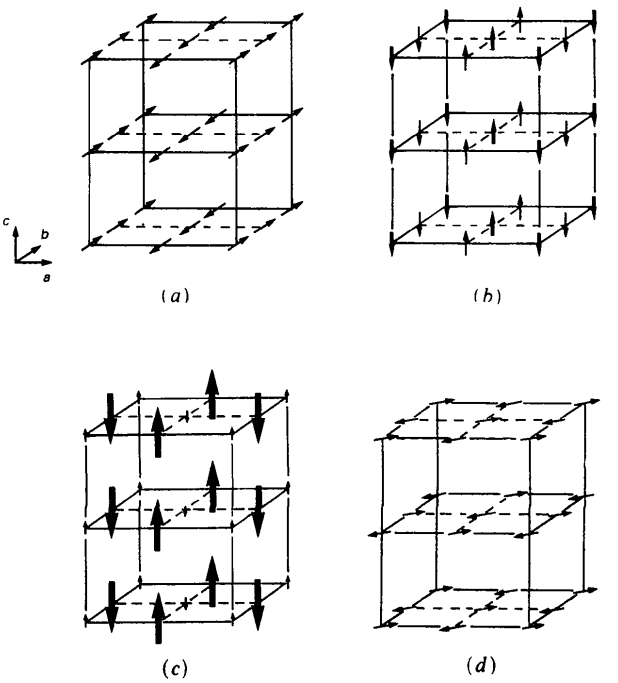

Fig. 6. Arrangement of the subcell dipoles for various experimentally observed tilting schemes for $RbVF_4$. The figures between brackets indicate the calculated subcell dipole moments in Cm units. (*a*) $\mathbf{a}_p^+\mathbf{a}_p^-\mathbf{c}^0$ ($14{\cdot}6\times10^{-30}$); (*b*) $\mathbf{a}_p^+\mathbf{a}^0\mathbf{c}^+$ ($12{\cdot}0\times10^{-30}$, $11{\cdot}3\times10^{-30}$); (*c*) $\mathbf{a}_p^+\mathbf{b}_p^+\mathbf{c}^+$ ($14{\cdot}4\times10^{-430}$); (*d*) $\mathbf{a}_a^-\mathbf{b}_a^-\mathbf{c}^-$ ($14{\cdot}0\times10^{-30}$).

Table 2. *List of the 75 possible ABX_4 structures as derived in the present work*

Symbol	Lattice centring	Unit-cell multiplicity	Z	Space group	No.	Diffraction typology
$\mathbf{a}^0\mathbf{a}^0\mathbf{c}^0$	P	$a\times b\times c$	1	$P4/mmm$	123	—
$\mathbf{a}_p^+\mathbf{a}^0\mathbf{c}^0$	P	$a\times 2b\times c$	2	$Pmmb$	51	Y
$\mathbf{a}_a^+\mathbf{a}^0\mathbf{c}^0$	A	$a\times 2b\times 2c$	4	$Ammm$	65	S
$\mathbf{a}_p^-\mathbf{a}^0\mathbf{c}^0$	C	$2a\times 2b\times c$	4	$Cmma$	67	M
$\mathbf{a}_a^-\mathbf{a}^0\mathbf{c}^0$	F	$2a\times 2b\times 2c$	8	$Fmmm$	69	A
$\mathbf{a}_p^+\mathbf{a}_p^+\mathbf{c}^0$	P	$2a\times 2b\times c$	4	$P4/nmm$	129	XYM
$\mathbf{a}_p^+\mathbf{b}_p^+\mathbf{c}^0$	P	$2a\times 2b\times c$	4	$Pmmn$	59	XYM
$\mathbf{a}_a^+\mathbf{a}_p^+\mathbf{c}^0$	A	$2a\times 2b\times 2c$	8	$Amma$	63	AXS
$\mathbf{a}_a^+\mathbf{b}_p^+\mathbf{c}^0$	A	$2a\times 2b\times 2c$	8	$Amma$	63	AXS
$\mathbf{a}_a^+\mathbf{a}_a^+\mathbf{c}^0$	I	$2a\times 2b\times 2c$	8	$I4/mmm$	139	RSM
$\mathbf{a}_a^+\mathbf{b}_a^+\mathbf{c}^0$	I	$2a\times 2b\times 2c$	8	$Immm$	71	RSM
$\mathbf{a}_p^-\mathbf{a}_p^-\mathbf{c}^0$	C	$2a\times 2b\times c$	4	$Pman$	53*	M
$\mathbf{a}_p^-\mathbf{b}_p^-\mathbf{c}^0$	C	$2a\times 2b\times c$	4	$C112/b$	13	M
$\mathbf{a}_p^-\mathbf{a}_a^-\mathbf{c}^0$	C	$2a\times 2b\times 2c$	8	$Cccb$	68	AZM
$\mathbf{a}_p^-\mathbf{b}_a^-\mathbf{c}^0$	C	$2a\times 2b\times 2c$	8	$Cccb$	68	AZM
$\mathbf{a}_a^-\mathbf{a}_a^-\mathbf{c}^0$	F	$2a\times 2b\times 2c$	8	$Ibmm$	74*	A
$\mathbf{a}_a^-\mathbf{b}_a^-\mathbf{c}^0$	F	$2a\times 2b\times 2c$	8	$F112/m$	12	A
$\mathbf{a}_p^+\mathbf{a}_p^-\mathbf{c}^0$	P	$2a\times 2b\times c$	4	$Pmab$	57	XYM
$\mathbf{a}_p^+\mathbf{b}_p^-\mathbf{c}^0$	P	$2a\times 2b\times c$	4	$Pmab$	57	XYM
$\mathbf{a}_a^+\mathbf{a}_p^-\mathbf{c}^0$	I	$2a\times 2b\times 2c$	8	$Imca$	72	RSM
$\mathbf{a}_a^+\mathbf{b}_p^-\mathbf{c}^0$	I	$2a\times 2b\times 2c$	8	$Imca$	72	RSM
$\mathbf{a}_p^+\mathbf{a}_a^-\mathbf{c}^0$	B	$2a\times 2b\times 2c$	8	$Bmab$	64	AYR
$\mathbf{a}_p^+\mathbf{b}_a^-\mathbf{c}^0$	B	$2a\times 2b\times 2c$	8	$Bmab$	64	AYR
$\mathbf{a}_a^+\mathbf{a}_a^-\mathbf{c}^0$	A	$2a\times 2b\times 2c$	8	$Amam$	63	AXS
$\mathbf{a}_a^+\mathbf{b}_a^-\mathbf{c}^0$	A	$2a\times 2b\times 2c$	8	$Amam$	63	AXS
$\mathbf{a}^0\mathbf{a}^0\mathbf{c}^+$	C	$2a\times 2b\times c$	4	$P4/mbm$	127*	M
$\mathbf{a}_p^+\mathbf{a}^0\mathbf{c}^+$	P	$2a\times 2b\times c$	4	$Pmmn$	59	XYM
$\mathbf{a}_a^+\mathbf{a}^0\mathbf{c}^+$	I	$2a\times 2b\times 2c$	8	$Immm$	71	RSM
$\mathbf{a}_p^-\mathbf{a}^0\mathbf{c}^+$	C	$2a\times 2b\times c$	4	$C12/m1$	12	M
$\mathbf{a}_a^-\mathbf{a}^0\mathbf{c}^+$	C	$2a\times 2b\times 2c$	8	$Ccmm$	63	AZM
$\mathbf{a}_p^+\mathbf{a}_p^+\mathbf{c}^+$	P	$2a\times 2b\times c$	4	$Pmmn$	59	XYM
$\mathbf{a}_p^+\mathbf{b}_p^+\mathbf{c}^+$	P	$2a\times 2b\times c$	4	$Pmmn$	59	XYM
$\mathbf{a}_a^+\mathbf{a}_p^+\mathbf{c}^+$	P	$2a\times 2b\times 2c$	8	$Pmmn$	59	$AXYRSM(Z)$
$\mathbf{a}_a^+\mathbf{b}_p^+\mathbf{c}^+$	P	$2a\times 2b\times 2c$	8	$Pmmn$	59	$AXYRSM(Z)$
$\mathbf{a}_a^+\mathbf{a}_a^+\mathbf{c}^+$	I	$2a\times 2b\times 2c$	8	$Immm$	71	RSM
$\mathbf{a}_a^+\mathbf{b}_a^+\mathbf{c}^+$	I	$2a\times 2b\times 2c$	8	$Immm$	71	RSM
$\mathbf{a}_p^-\mathbf{a}_p^-\mathbf{c}^+$	C	$2a\times 2b\times c$	4	$P2/b11$	13*	M
$\mathbf{a}_p^-\mathbf{b}_p^-\mathbf{c}^+$	C	$2a\times 2b\times c$	4	$P\bar{1}$	2*	M
$\mathbf{a}_a^-\mathbf{a}_p^-\mathbf{c}^+$	C	$2a\times 2b\times 2c$	8	$C12/c1$	15	AZM
$\mathbf{a}_a^-\mathbf{b}_p^-\mathbf{c}^+$	C	$2a\times 2b\times 2c$	8	$C12/c1$	15	AZM
$\mathbf{a}_a^-\mathbf{a}_a^-\mathbf{c}^+$	C	$2a\times 2b\times 2c$	8	$Pbnm$	62*	AZM
$\mathbf{a}_a^-\mathbf{b}_a^-\mathbf{c}^+$	C	$2a\times 2b\times 2c$	8	$P112_1/m$	11*	AZM
$\mathbf{a}_p^+\mathbf{a}_p^-\mathbf{c}^+$	P	$2a\times 2b\times c$	4	$P2_1/m11$	11	XYM
$\mathbf{a}_p^+\mathbf{b}_p^-\mathbf{c}^+$	P	$2a\times 2b\times c$	4	$P2_1/m11$	11	XYM
$\mathbf{a}_a^+\mathbf{a}_p^-\mathbf{c}^+$	I	$2a\times 2b\times 2c$	8	$I2/m11$	12	RSM
$\mathbf{a}_a^+\mathbf{b}_p^-\mathbf{c}^+$	I	$2a\times 2b\times 2c$	8	$I2/m11$	12	RSM
$\mathbf{a}_p^+\mathbf{a}_a^-\mathbf{c}^+$	P	$2a\times 2b\times 2c$	8	$Pmcn$	62	$AXYZRM(S)$
$\mathbf{a}_p^+\mathbf{b}_a^-\mathbf{c}^+$	P	$2a\times 2b\times 2c$	8	$Pmcn$	62	$AXYZRM(S)$
$\mathbf{a}_a^+\mathbf{a}_a^-\mathbf{a}^+$	P	$2a\times 2b\times 2c$	8	$Pmnm$	59	$AXZRSM(Y)$
$\mathbf{a}_a^+\mathbf{b}_a^-\mathbf{c}^+$	P	$2a\times 2b\times 2c$	8	$Pmnm$	59	$AXZRSM(Y)$
$\mathbf{a}^0\mathbf{a}^0\mathbf{c}^-$	F	$2a\times 2b\times 2c$	8	$F4/mmc$	140	A
$\mathbf{a}_p^+\mathbf{a}^0\mathbf{c}^-$	B	$2a\times 2b\times 2c$	8	$Bmmb$	63	AYR
$\mathbf{a}_a^+\mathbf{a}^0\mathbf{c}^-$	A	$2a\times 2b\times 2c$	8	$Amma$	63	AXS
$\mathbf{a}_p^-\mathbf{a}^0\mathbf{c}^-$	C	$2a\times 2b\times 2c$	8	$Ccmb$	64	AZM
$\mathbf{a}_a^-\mathbf{a}^0\mathbf{c}^-$	F	$2a\times 2b\times 2c$	8	$F12/m1$	12	A
$\mathbf{a}_p^+\mathbf{a}_p^+\mathbf{c}^-$	P	$2a\times 2b\times 2c$	8	$Pmmn$	59	$AXYRSM(Z)$
$\mathbf{a}_p^+\mathbf{b}_p^+\mathbf{c}^-$	P	$2a\times 2b\times 2c$	8	$Pmmn$	59	$AXYRSM(Z)$
$\mathbf{a}_a^+\mathbf{a}_p^+\mathbf{c}^-$	A	$2a\times 2b\times 2c$	8	$Amma$	63	AXS
$\mathbf{a}_a^+\mathbf{b}_p^+\mathbf{c}^-$	A	$2a\times 2b\times 2c$	8	$Amma$	63	AXS
$\mathbf{a}_a^+\mathbf{a}_a^+\mathbf{c}^-$	P	$2a\times 2b\times 2c$	8	$Pmmn$	59	$AXYRSM$
$\mathbf{a}_a^+\mathbf{b}_a^+\mathbf{c}^-$	P	$2a\times 2b\times 2c$	8	$Pmmn$	59	$AXYRSM$
$\mathbf{a}_p^-\mathbf{a}_p^-\mathbf{c}^-$	C	$2a\times 2b\times 2c$	8	$Pcan$	60*	AZM
$\mathbf{a}_p^-\mathbf{b}_p^-\mathbf{c}^-$	C	$2a\times 2b\times 2c$	8	$P112_1/n$	14*	AZM
$\mathbf{a}_p^-\mathbf{a}_a^-\mathbf{c}^-$	C	$2a\times 2b\times 2c$	8	$C12/c1$	15	AZM
$\mathbf{a}_p^-\mathbf{b}_a^-\mathbf{c}^-$	C	$2a\times 2b\times 2c$	8	$C12/c1$	15	AZM

Table 2 (*cont.*)

Symbol	Lattice centring	Unit-cell multiplicity	Z	Space group	No.	Diffraction typology
$\mathbf{a}_a^-\mathbf{a}_a^-\mathbf{c}^-$	F	$2a\times2b\times2c$	8	$I2/b11$	15*	A
$\mathbf{a}_a^-\mathbf{b}_a^-\mathbf{c}^-$	F	$2a\times2b\times2c$	8	$I\bar{1}$	2*	A
$\mathbf{a}_p^+\mathbf{a}_p^-\mathbf{c}^-$	P	$2a\times2b\times2c$	8	$Pmnb$	62	$AXYZRM(S)$
$\mathbf{a}_p^+\mathbf{b}_p^-\mathbf{c}^-$	P	$2a\times2b\times2c$	8	$Pmnb$	62	$AXYZRM(S)$
$\mathbf{a}_a^+\mathbf{a}_p^-\mathbf{c}^-$	P	$2a\times2b\times2c$	8	$Pmca$	57	$AXZRSM(Y)$
$\mathbf{a}_a^+\mathbf{b}_p^-\mathbf{c}^-$	P	$2a\times2b\times2c$	8	$Pmca$	57	$AXZRSM(Y)$
$\mathbf{a}_p^+\mathbf{a}_a^-\mathbf{c}^-$	B	$2a\times2b\times2c$	8	$B2/m11$	12	AYR
$\mathbf{a}_p^+\mathbf{b}_a^-\mathbf{c}^-$	B	$2a\times2b\times2c$	8	$B2/m11$	12	AYR
$\mathbf{a}_a^+\mathbf{a}_a^-\mathbf{c}^-$	A	$2a\times2b\times2c$	8	$A2_1/m11$	11	AXS
$\mathbf{a}_a^+\mathbf{b}_a^-\mathbf{c}^-$	A	$2a\times2b\times2c$	8	$A2_1/m11$	11	AXS

* These space-group symbols refer to axes chosen according to the matrix transformation

$$\begin{pmatrix} \frac{1}{2} & \frac{1}{2} & 0 \\ \frac{1}{2} & -\frac{1}{2} & 0 \\ 0 & 0 & 1 \end{pmatrix}.$$

(*d*) *Complete list of hettotype structures*

The complete list is shown in Table 2 and contains information about all generated phases.

The lattice centring, unit-cell multiplicity and Z, the number of octahedra contained in it, are all referred to a new unit cell expressed in terms of the lattice parameters of the aristotype (*i.e.* the basic translations have to be taken along the former tetragonal axes *a*, *b*, *c* of the aristotype).

It should be noticed that the possibilities of the international Hermann–Mauguin symbols for space groups are exploited at a maximum in order to avoid any unnecessary changes of the axial setting. This will be of great help when the group-to-subgroup relations have to be established.

Sometimes, however, a transformation of the type

$$\begin{bmatrix} \frac{1}{2} & -\frac{1}{2} & 0 \\ \frac{1}{2} & \frac{1}{2} & 0 \\ 0 & 0 & 1 \end{bmatrix} \qquad (5)$$

is necessary and those space groups referring to axes transformed according to (5) have been labelled with an asterisk.

For the diffraction typology, the supplementary superstructure reflections due to the A-cation displacements are added in brackets. It is noticeable that it is only in a few cases with positive and negative tilt correlation along [001] that these supplementary reflections appear.

A brief survey of some already determined ABX_4 phases is given in Table 3. Here, use is made of the structure symbol for ABX_4 structures and whenever necessary the data provided by the authors were used to determine or extend it properly. Space-group symbols marked with an asterisk again refer to axes chosen according to the matrix transformation (5). The complete list of hettotype structures was presented at the XIIIth International Congress of

Table 3. *Survey of already determined ABX_4 structures*

In the case of Hidaka, Wood & Garrard (1979), Hidaka, Wood, Wanklyn & Garrard (1979), Hidaka, Wood & Wondre (1979) and Hidaka *et al.* (1982),the data provided by the authors were used to establish the structure symbol. Also the observed space group is compared with the space group of the tilted octahedral framework.

Material	Phase	Symbol	Space group observed	Space group framework	Reference
$CsVF_4$	(III)	$\mathbf{a}_p^+\mathbf{b}_p^+\mathbf{c}^+$	$Pmmn$	$Pmmn$	(*a*)
	(II)	$\mathbf{a}^0\mathbf{a}_p^+\mathbf{c}^0$	$Pmma$	$Pmma$	(*a*)
	(I)	$\mathbf{a}^0\mathbf{a}^0\mathbf{c}^0$	$P4/mmm$	$P4/mmm$	(*a*)
$CsFeF_4$	(IV)	$\left\{\begin{matrix}\mathbf{a}_p^+\mathbf{b}_p^+\mathbf{c}^0\\ \mathbf{a}_p^+\mathbf{b}_p^+\mathbf{c}^+\end{matrix}\right\}$	$P2_12_12$	$Pmmn$	(*b*)(*c*)
	(III)	$\mathbf{a}_p^+\mathbf{b}_p^+\mathbf{c}^+$	$Pmmn$	$Pmmn$	(*b*)(*c*)
	(III)	$\mathbf{a}_p^+\mathbf{a}_p^-\mathbf{c}^0$	$Pmab$	$Pmab$	(*d*)
	(III)	$\mathbf{a}_p^+\mathbf{a}_p^+\mathbf{c}^0$	$P4/nmm$	$P4/nmm$	(*e*)
	(II)	$\mathbf{a}^0\mathbf{a}_p^+\mathbf{c}^0$	$Pmma$	$Pmma$	(*b*)(*c*)
	(I)	$\mathbf{a}^0\mathbf{a}^0\mathbf{c}^0$	$P4/mmm$	$P4/mmm$	(*b*)(*c*)
$RbFeF_4$	(III)	$\mathbf{a}_p^+\mathbf{a}_p^-\mathbf{c}^0$	$Pmab$	$Pmab$	(*d*)
	(III)	$\left\{\begin{matrix}\mathbf{a}_p^+\mathbf{b}_p^+\mathbf{c}^0\\ \mathbf{a}_p^+\mathbf{b}_p^+\mathbf{c}^+\end{matrix}\right\}$	$P2_12_12$	$Pmmn$	(*b*)
	(II)	$\mathbf{a}^0\mathbf{a}_p^+\mathbf{c}^0$	$Pmma$	$Pmma$	(*b*)
	(I)	$\mathbf{a}^0\mathbf{a}^0\mathbf{c}^0$	$P4/mmm$	$P4/mmm$	(*b*)
$RbVF_4$	(V)	$\mathbf{a}_p^+\mathbf{b}_p^+\mathbf{c}^+$	$P2_12_12$	$Pmmn$	(*f*)
	(IV)	$\mathbf{a}_a^+\mathbf{b}_a^-\mathbf{c}^+$	$P2_12_12_1$	$Pmnm$	(*f*)
	(III)	$\mathbf{a}_p^+\mathbf{a}^0\mathbf{c}^+$	$Pmmn$	$Pmmn$	(*f*)
	(II)	$\mathbf{a}^0\mathbf{a}^0\mathbf{c}^+$	$C4/mbm$	$C4/mbm$	(*f*)
$RbAlF_4$	(III)	$\mathbf{a}_p^+\mathbf{b}_p^+\mathbf{c}^+$	$Pmmn$	$Pmmn$	(*g*)
	(II)	$\mathbf{a}^0\mathbf{a}^0\mathbf{c}^+$	$C4/mbm$	$C4/mbm$	(*g*)
	(I)	$\mathbf{a}^0\mathbf{a}^0\mathbf{c}^0$	$P4/mmm$	$P4/mmm$	(*g*)
$TlAlF_4$	(III)	$\mathbf{a}_a^-\mathbf{a}_a^-\mathbf{c}^-$	$C2/m$	$I12/a\,1$*	(*g*)
	(II)	$\mathbf{a}^0\mathbf{a}^0\mathbf{c}^-$	$I4/mcm$	$I4/mcm$	(*g*)
	(I)	$\mathbf{a}^0\mathbf{a}^0\mathbf{c}^0$	$P4/mmm$	$P4/mmm$	(*g*)
$KAlF_4$	(II)	$\mathbf{a}^0\mathbf{a}^0\mathbf{c}^+$	$C4/mbm$	$C4/mbm$	(*g*)
NH_4AlF_4	(II)	$\mathbf{a}^0\mathbf{a}^0\mathbf{c}^-$	$F4/mcm$	$F4/mcm$	(*g*)

References: (*a*) Hidaka, Wood & Garrard (1979); (*b*) Hidaka, Wood, Wanklyn & Garrard (1979); (*c*) Hidaka, Wood & Wondre (1979); (*d*) Abrahams & Bernstein (1972); (*e*) Babel, Wall & Heger (1974); (*f*) Hidaka, Inoue, Garrard & Wanklyn (1982); (*g*) Bulou *et al.* (1983).

* This space-group symbol refers to axes chosen according to the matrix transformation

$$\begin{pmatrix} \frac{1}{2} & \frac{1}{2} & 0 \\ \frac{1}{2} & -\frac{1}{2} & 0 \\ 0 & 0 & 1 \end{pmatrix}.$$

Crystallography, Hamburg (Deblieck, Van Landuyt & Amelinckx, 1984). Since it is technically impossible to publish some of the results of this work *in extenso*, complete printouts containing coordinates, structure factors, *A*-cation displacements and subcell dipole data for specific compositions and tilt angles are available at the authors' laboratory.

Recently, the complete list was used in order to interpret the experimental results of an electron microscopic study of $RbVF_4$ and $RbFeF_4$ (Deblieck, Van Landuyt, Garrard, Wanklyn & Amelinckx, 1984; Deblieck, Van Landuyt & Amelinckx, 1985).

4. Group-to-subgroup relations

As previously mentioned it is useful to have a closer look at the group-to-subgroup relations because they allow a better understanding of the symmetry dependence between the structures of the aristotype and its hettotypes, especially when the study of phase transitions is aimed at.

Bärnighausen (1975, 1980) introduced the concept of a '*Stammbaum*' or 'family tree' by which it is possible to get a complete overview of the symmetry relations between all members of a family of struc-

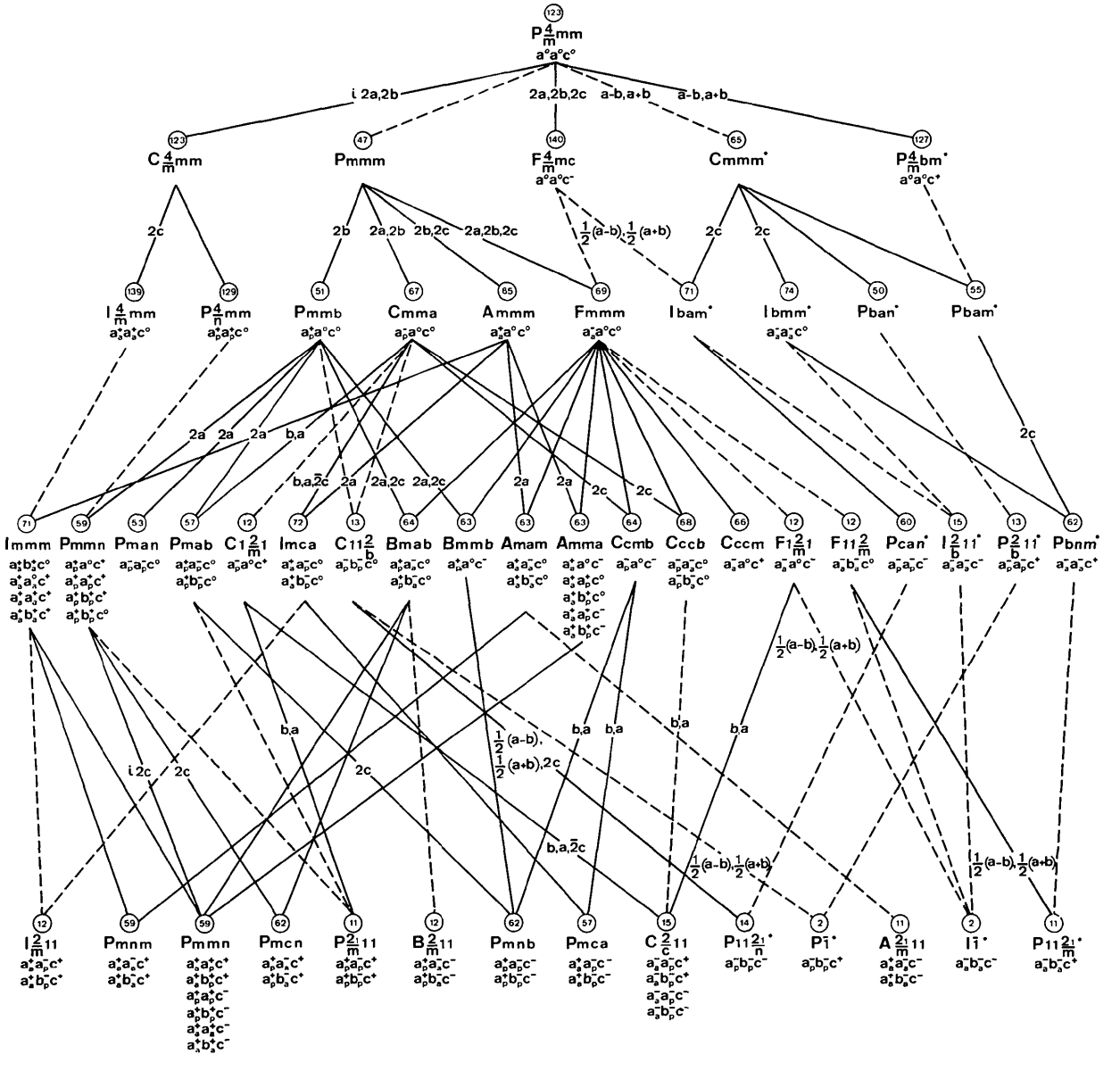

Fig. 7. Family tree of the 75 possible ABX_4 structures as derived in the present work. The space groups labelled with a dot refer to axes chosen according to the transformation (5).

tures, since in general the different phases of a particular compound are symmetry related.

It has to be emphasized, however, that the mere existence of a symmetry relationship between two phases does not automatically imply that a phase transition is possible. In fact it proves to be necessary, in general, to check on the Landau criteria to point out whether an actual relationship between the structural symmetry of two phases also stands for a physical transition.

Furthermore the symmetry relationships between experimentally observed phases are not necessarily the product of one symmetry-reducing mechanism as is the case here.

The Bärnighausen family tree consists of 'equisymmetrical' levels, on which all phases with the same number of symmetry elements are indicated with their space group, structure and phase indication (*e.g.* α-$NaTiF_4$). The aristotype structure will obviously occupy the highest level since it possesses the highest symmetry allowed. In between the levels, the symmetry reductions between single phases are symbolized by arrows, which carry information on the type and index of the symmetry reduction and, if necessary, transformation of the unit cell.

Three types of symmetry reduction are discerned:

(i) isomorphic (*i*);

(ii) *klassengleiche* (*k*);

(iii) *translationengleiche* (*t*).

In isomorphic symmetry reductions the space group of the higher symmetric phases G_0 is equivalent to the space group of the lower symmetric phase *H*.

For *klassengleiche* symmetry reductions the point group is conserved in the descent but translation symmetry is lost, whereas for the *translationengleiche* reductions the translation symmetry is conserved but the point group is reduced in symmetry. The index *n* of the symmetry reduction is defined as:

$$n = |G_0|/|H|,$$

where $|G_0|$ and $|H|$ represent the order of the group G_0 and its maximal subgroup *H*, respectively.

The group-to-subgroup relation between a particular group and its maximal subgroups (*i.e.* subgroups of lowest index) can be derived by the use of the character tables of the space groups; however, much redundant labour is avoided by using the tables of Neubüser & Wondratschek (1966), which give all maximal subgroups, classified according to the type of symmetry reduction involved with their index and necessary unit-cell adaptations for a particular space group. These tables have been incorporated in *International Tables for Crystallography* (1983) and they have also been inverted so that the minimal supergroups for each particular space group can be obtained.

The family tree of all 74 ABX_4 hettotype structures contained in the complete list, derived from the aristotype by the previously described symmetry reducing mechanism, is shown in Fig. 7 in a presentation that is optimized for conciseness. The structure symbol takes the place of the structure and phase indication; the number of the space group is encircled. All symmetry reductions are of index 2; therefore the index is omitted. The *klassengleiche* reductions are marked by full lines, the *translationengleiche* reductions are in broken lines whereas the isomorphic reductions are represented by full lines carrying an index *i*.

Necessary unit-cell transformations are given by the lattice parameters involved (*i.e.* if a lattice parameter is not mentioned it remains unchanged).

This family tree can be compared with the family tree of experimentally observed ABX_4 structures

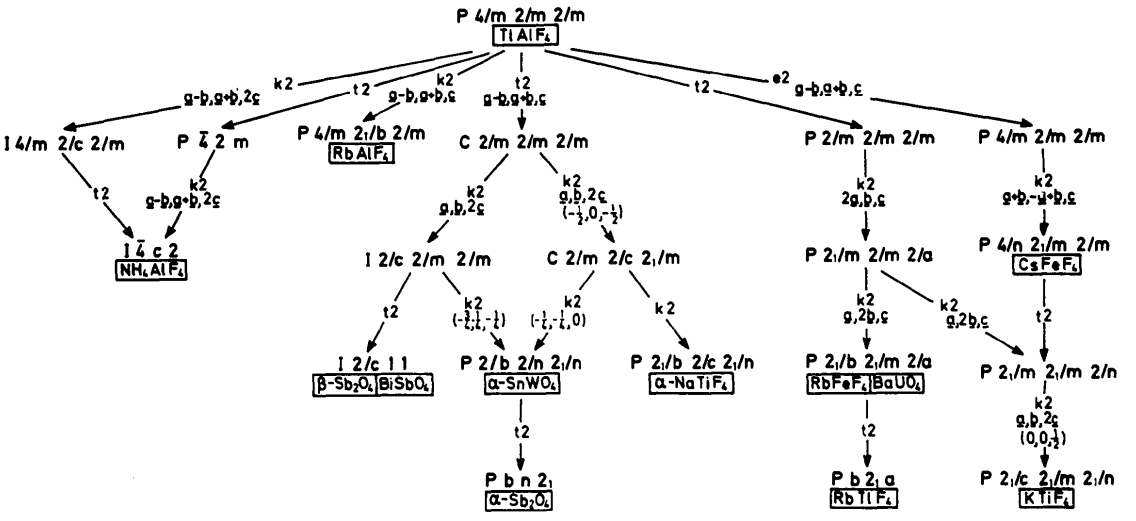

Fig. 8. Family tree of experimentally observed ABX_4 structures. (Courtesy: H. Bärnighausen.)

(Meyer, 1981), which is shown in Fig. 8. The two family trees are related to the extent that the only descent in symmetry they can have in common must be caused solely by the tilting of rigid octahedra.

It must be mentioned that a family tree of $RbAlF_4$ and $RbVF_4$, whereby the maximal subgroups are derived by making use of a decomposition of the factor groups, was recently published (Loyzance & Couzy, 1984). This family tree, however, is restricted to one line of descent along the space groups of the phases involved in observed transitions in $RbAlFe_4$ and $RbVF_4$:

$$P4/m\,mm \rightarrow P4/m\,bm \rightarrow Pmmn \rightarrow P2_12_12_1 \rightarrow P2_12_12$$

and is therefore of a different kind from the present one shown in Fig. 7 which considers all possible lines of descent but is restricted to a particular mechanism of symmetry reduction.

5. Concluding remarks

The present work is meant as a practical and useful guide for scientists involved in the field of structural investigation of the low-temperature phases and phase transitions between them, in the perovskite-like ABX_4 case.

As for the use of this formalism in the field of phase transitions, more specifically the part on group-to-subgroup relations, it must be emphasized that additional calculations based on Landau theory may be necessary to find out whether a transition is physically feasible.

References

ABRAHAMS, S. C. & BERNSTEIN, J. L. (1972). *Mater. Res. Bull.* **7**, 715–720.

AHTEE, M., GLAZER, A. M. & MEGAW, H. D. (1972). *Philos. Mag.* **26**, 995–1014.

BABEL, D., WALL, F. & HEGER, G. (1974). *Z. Naturforsch. Teil B*, **29**, 139–148.

BÄRNIGHAUSEN, H. (1975). *Acta Cryst.* A**31**, S3.

BÄRNIGHAUSEN, H. (1980). *Math. Chem.* **9**, 139–175.

BULOU, A., FOURQUET, J. L., LEBLE, A., NOUET, J., DE PAPE, R. & PLET, F. (1983). *Solid State Chemistry. Proc. 2nd Eur. Conf.* edited by R. METSELAAR, H. J. HEIJLIGERS & J. SCHOONMAN, pp. 679–682. Amsterdam: Elsevier Scientific.

DEBLIECK, R., VAN LANDUYT, J. & AMELINCKX, S. (1984). *Acta Cryst.* A**40**, C211.

DEBLIECK, R., VAN LANDUYT, J. & AMELINCKX, S. (1985). Accepted for publication in *J. Solid State Chem.*

DEBLIECK, R., VAN LANDUYT, J., GARRARD, B. J., WANKLYN, B. M. R. & AMELINCKX, S. (1984). *Acta Cryst.* A**40**, C129.

GLAZER, A. M. (1972). *Acta Cryst.* B**28**, 3384–3392.

GLAZER, A. M. (1975). *Acta Cryst.* A**31**, 756–762.

GUPTA, C. L., PANDE, M. K., SHUKLA, D. D. & SHARMA, M. N. (1980). *J. Phys. Soc. Jpn.*, **48**, 384–390.

HIDAKA, M., INOUE, K., GARRARD, B. J. & WANKLYN, B. M. (1982). *Phys. Status Solidi A*, **72**, 809–816.

HIDAKA, M., WOOD, I. G. & GARRARD, B. J. (1979). *Phys. Status Solidi A*, **56**, 349–354.

HIDAKA, M., WOOD, I. G., WANKLYN, B. M. R. & GARRARD, B. J. (1979). *J. Phys. C*, **12**, 1799–1807.

HIDAKA, M., WOOD, I. G. & WONDRE, F. R. (1979). *J. Phys. C*, **12**, 4179–4183.

International Tables for Crystallography (1983). Vol. *A*. Dordrecht: Reidel.

KAY, H. F. & BAILEY, P. C. (1957). *Acta Cryst.* **10**, 219–226.

LOYZANCE, P. L. & COUZI, M. (1984). *Phys. Status Solidi A*, **85**, 359–374.

MEGAW, H. D. (1973). *Crystal Structures. A Working Approach.* Philadelphia: Saunders.

MEYER, A. (1981). PhD Thesis, Karlsruhe.

NEUBÜSER, J. & WONDRATSCHEK, H. (1966). *Krist. Tech.* **1**, 529–543.

UPADHYAYA, J. C., WANG, S. & MOORE, R. A. (1980). *Can J. Phys.* **58**, 905–911.